High Performance Selective and Output Filter Techniques for Sensorless Direct Position and Speed Estimation

Matthias Preindl, *IEEE Senior Member*

***Abstract*—This work introduces high performance filter techniques for direct position and speed estimation to augment its robustness against disturbances. The direct estimation concept provides an independent position and speed estimate at each sampling instant by solving an optimization problem parameterized with the current, current derivative, and voltage of the same sample. It can operate at any speed employing a voltage injection at low speed or PWM current derivative. A selective filter concept is proposed that discards samples lacking robustness based on cost function properties. The concept is most effective in removing worst case errors and should always be applied. Also, output filter techniques are investigated to improve the estimates. A finite impulse response (FIR) structure is proposed that filters estimates according to a least-square criterion and is effective in reducing average estimation errors. The FIR filter is benchmarked against an enhanced dual-PLL filter, which is enabled by direct estimation. The FIR and dual-PLL filters are found to have a 6.8kHz and 1kHz practical bandwidth, respectively, while achieving a <1% absolute mean position and speed estimation error. Hence, they perform one to two orders of magnitude better than traditional estimation schemes, which typically achieve <100Hz bandwidth at similar errors.**

***Index Terms*—Estimation, Motor Drives, Numerical Stability, Optimization Methods, Robustness**

I. Introduction

SYNCHRONOUS motor drives require an accurate rotor position and speed information for high performance control. Position sensorless estimation schemes have been introduced to remove the cost of a resolver or encoder and improve their reliability by removing a single point of failure. These arguments are especially compelling in mass-produced drive systems, e.g. in hybrid and electric vehicles, when the machine is physically distant from the motor controller, e.g. pumps for underground mining or wind power plants with converter at the tower base, the available space for a motor drive is restricted, e.g. low power drives, or a drive system operates in hazardous or clean environments, where physical contact between stator and rotor is undesired.

Position sensorless estimation schemes are typically classified in high speed methods and zero speed methods. High-speed methods use predominantly the back-EMF information [1]–[4] and can be formulated as flux observers [5], [6], sliding mode observers [7], [8], extended Kalman filters (EKF) [9], [10], and adaptive observers [11], [12]. Zero speed methods introduce a perturbation to identify the rotor position in anisotropic machines. Estimation schemes for PWM control inject a high frequency signal and demodulate the machine response for rotor position information using filters [13]–[15]. Direct motor control schemes without PWM require dedicated implementations that can exploit the current ripple [16], [17]. These estimation methods can be combined to achieve position sensorless control at any speed but require a cross-over between the zero and high speed method [18], [19], which can be challenging during fast transients. Finally, even methods intended for highly dynamic conditions require filtering by limiting the estimation gains [20] or a *phase-locked loop* (PLL) [3] for stable operation. In literature, the bandwidth of position sensorless strategies is often not specified. Where it is provided, it ranges typically between 20-50Hz and rarely exceeds 100Hz by a relevant margin [3], [13]–[15], [21]. This paper proposes strategies to significantly improve the dynamic capabilities of position sensorless estimation while retaining a low error due to disturbances.

Direct position and speed sensorless estimation obtains an independent position and speed estimate by solving a nonlinear optimization problem. The concept is based on [22], [23] (without PLL filters), that yields: (i) "instantaneous" estimation by extracting a position and speed estimate from the measurements of one sample (two samples if the current derivative is computed from two adjacent samples), (ii) a single scheme for low and high speed position estimation, (iii) compatibility with any perturbation, i.e. any signal injection technique or exploiting the current ripple, for low speed estimation, (iv) compatibility with nonlinear motor models that account for saturation. The concept consists in identifying the position and speed based on a least squares formulation of the dynamic model parametrized with the measurements of one sample. The resulting cost function is nonlinear in the estimates and is solved numerically in real time. This approach (with added PLL filtering) has been studied for applications that require high dynamic torque control, e.g. belt-starter-generator drives that must crank an engine or electric vehicle traction motor drives. It was combined with PWM control, e.g. vector control or convex control set model predictive control (CCS-MPC) [22], which uses a high frequency perturbation for low speed estimation, and direct control, e.g. finite control set model predictive control (FCS-MPC) [23], which uses the inherent random switching ripple for low speed estimation. It can also take magnetic saturation into account [24] and can be applied to induction motors [25]. A block diagrams is shown in Fig. 1.

This paper studies filter strategies for direct position estimation since its inherent noise behavior may not be acceptable for some applications [26]–[28]. Initially, it is shown empirically that the direct estimation robustness against disturbances depends on the robustness factor ρ, which describes the convexity of the cost function. The nonlinear cost function is time-varying since it is parameterized at each time instant with the motor currents and terminal voltage. If it lacks convexity, even limited noise can result in large estimation errors. We show that the robustness factor is typically high at high speed. At low speed, the robustness factor tends to zero unless a perturbation strategy is used to

Manuscript received February 17, 2019; revised May 23, 2019; revised September 15, 2019; accepted October 27, 2019.

Matthias Preindl is with Department of Electrical Engineering, Columbia University in the City of New York, New York, NY 10027, USA (e-mail: matthias.preindl@gmail.com).

maintain a minimum value (on average). However, it is difficult to guarantee a minimum robustness factor. Hence, a *selective filter strategy* is proposed that discards samples below a threshold, i.e. minimum robustness factor. This concept is shown to be most effective to discard the worst case samples and a small threshold should always be applied. Increasing the threshold value eventually becomes ineffective. At even higher thresholds, selective filtering may discard a large number or even majority of the estimates and the estimation process deteriorates rapidly.

Since direct estimation issues an independent position and speed estimates at each time instant, *output filter strategies* can be applied that reduce noise by linking an estimate to past N estimates. A *finite impulse response* (FIR) filter is proposed that solves a least-squares statement. First, the filter fits the position and speed estimate to the equation $\dot{\theta} = \omega$, which is not guaranteed by direct estimation. Second, the speed is assumed to vary at most linearly over the past N samples, which holds assuming that N is reasonably small. Based on these conditions, the FIR filter interpolates a position and speed sequence in the least-squares sense. The result is shown to decrease estimation noise with no compromise in terms of dynamics up to $N = 5$ and a limited decrease of dynamic performance at higher N. Furthermore, a dual-PLL concept is proposed, which uses a second parallel speed loop enabled by the independent speed estimate of direct estimation. The concept is derived from dual-PLL strategies that improve the position measurement quality of (low resolution) encoders [29], [30] or remove harmonics [31]. The dual-PLL has a 1kHz estimation bandwidth, which is more than a factor 10 higher than a conventional PLL (50Hz [22], [23]). It acts as a benchmark reference to the FIR filter, which achieves a 6.8kHz bandwidth at similar absolute mean estimation errors (<1%).

This paper is organized a follows. The direct position and speed estimation concept is introduced in Section II. The output filtering concepts are discussed in Section III and the filters are evaluated in Section IV.

II. Direct Position and Speed Estimation

A. Direct Estimation Concept

Direct parameter estimation targets the estimation of the unknown parameters $z \in \mathbb{Z} \subseteq \mathbb{R}^l$ from the nonlinear dynamic system $\dot{x} = f(x, u, z) + w$, with states $x \in \mathbb{X} \subseteq \mathbb{R}^n$ and inputs $u \in \mathbb{U} \subseteq \mathbb{R}^m$ in presence of an unknown bounded disturbance $w \in \mathbb{W} = \{w \in \mathbb{R}^2 \mid \|w\| \leq W\}$ at time instant t. For simplicity of notation, this paper refers to a continuous-time derivative $\dot{x}$, which is obtained from two adjacent x in sampled systems. We assume that $f : \mathbb{X} \times \mathbb{U} \times \mathbb{Z} \times \mathbb{W} \to \mathbb{R}^n$ is smooth and the sets $\mathbb{X}$, $\mathbb{U}$, $\mathbb{Z}$, and $\mathbb{W}$ are convex. Direct estimation uses the known states x and inputs u to generate an estimate $\hat{z} = z + \tilde{z}$, where $\tilde{z}$ is the estimation error. The residuals of the dynamic system

$$r(\hat{z}) = f(x, u, \hat{z}) - \dot{x} + w, \tag{1}$$

act as a qualifier of an estimate $\hat{z}$. For $w = 0$, $r(\hat{z}) = 0$ is a *necessary* condition such that $\hat{z} = z$, i.e. $\tilde{z} = 0$. In these conditions, $\hat{z} = z$ implies $r(\hat{z}) = 0$ but the reverse is not true in general and additional provisions are necessary. Since $w \neq 0$,

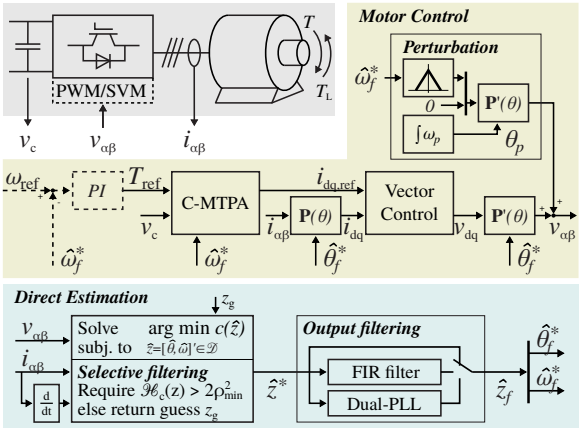

Fig. 1. Vector control (with Constrained-MTPA [33]) using direct position and speed estimation (an optional external speed-loop can be added). A rotating high-frequency voltage perturbation is added at low speeds. the perturbation magnitude is linearly scaled to zero as the speed magnitude increases.

direct parameter estimation fits the parameters in a nonlinear least squares sense with the optimization problem

$$\hat{z}^\star = \arg\min_{\hat{z} \in \mathcal{D}} c(\hat{z}) = \|r(\hat{z})\|^2 = r(\hat{z})' r(\hat{z}), \tag{2}$$

with cost function $c : \mathbb{Z} \to \mathbb{R}$ and search domain $\mathcal{D} \subseteq \mathbb{Z}$. At the time of solving (2), w is unknown and assumed to be zero.

For estimation purposes the optimizer $\hat{z}^\star$ has to be unique, which is provided if $c(\hat{z})$ is strictly convex on $\mathcal{D}$ [32]. In these conditions, $\hat{z}^\star = z$ assuming that $w = 0$. Any disturbance $w \neq 0$ will inevitably result in a nonzero estimation error, i.e. $\|\hat{z}^\star - z\| > 0$. However, it can be shown that $\|\hat{z}^\star - z\| < Z_w$ for any bounded disturbance $\|w\| < W$ if $c(\hat{z})$ is strictly convex on $\mathcal{D}$. The search domain $\mathcal{D}$ can be computed explicitly but the required programs are np-hard for nonlinear systems in general. Hence, its computation can be replaced with convexity checks in real-time implementations.

B. Synchronous Machine Model

For control purposes, the armature (stator) flux and currents of synchronous machines, i.e. permanent magnet (PMSM), wound-rotor (without damper windings), and reluctance machines (RSM) is linked using the dq reference frame [33], [34]

$$\lambda_{dq} = l \circ i_{dq} \approx \mathbf{L} i_{dq} + \psi_r, \tag{3}$$

where $l : \mathbb{R}^2 \to \mathbb{R}^2$ is the nonlinear map that links dq current and flux globally. The nonlinear map can be computed using finite element analysis (FEA) or measured experimentally. For control purposes, this relation is often approximated by an affine map with parameters $\mathbf{L} = \mathrm{diag}[L_d, L_q]$ and $\psi_r = [\psi, 0]'$, where L_d and L_q are the d and q axis inductances and ψ is the rotor flux magnitude, and $'$ denotes the transpose operator. We assume that the affine approximation is a fit with reasonable accuracy, e.g. using optimized parameters [33].

The implicit position dependence of the dq reference frame is made explicit by transforming into the static $\alpha\beta$ system with the Park transformation $\mathbf{P}(\theta) = [[\cos\theta, -\sin\theta]', [\sin\theta, \cos\theta]']$, which is orthogonal ($\mathbf{P}^{-1}(\theta) = \mathbf{P}'(\theta)$),

$$\lambda_{\alpha\beta} = \mathbf{P}'(\theta)\mathbf{L}\mathbf{P}(\theta) i_{\alpha\beta} + \mathbf{P}'(\theta)\psi_r. \tag{4}$$

where $\lambda_{dq} = \mathbf{P}(\theta)\lambda_{\alpha\beta}$ and $i_{dq} = \mathbf{P}(\theta)i_{\alpha\beta}$. Deriving this expression with respect to time results in the dynamic synchronous machine model

$$\bar{v}_{\alpha\beta} = \left(L_\Sigma \mathbf{I} + L_\Delta \bar{\mathbf{P}}(2\theta)\right)\dot{i}_{\alpha\beta} + 2L_\Delta \omega \mathbf{J}\bar{\mathbf{P}}(2\theta)i_{\alpha\beta} + \omega \mathbf{J}\mathbf{P}(\theta)'\psi_r, \tag{5}$$

where $L_\Sigma = (L_d + L_q)/2$ and $L_\Delta = (L_d - L_q)/2$ is the sum and difference inductance [22], respectively. The compensated terminal voltage $\bar{v}_{\alpha\beta} = \dot{\lambda}_{\alpha\beta} = v_{\alpha\beta} - \Delta v_{\alpha\beta}$ is the terminal voltage applied by control $v_{\alpha\beta}$ compensated with the effective voltage drop $\Delta v_{\alpha\beta}$ due to the stator resistance, inverter on-voltage drops, and dead-times [34]. The $\Delta v_{\alpha\beta}$ term is related to the power losses in the current conduction path. It is typically a few percent of $v_{\alpha\beta}$ and can be approximated with lookup tables or analytical models [34] without knowledge of θ or ω. The matrices $\mathbf{J} = [[0,1]', [-1,0]']$ is a $\pi/2$ rotation, $\bar{\mathbf{I}} = [[1,0]', [0,-1]']$, and $\bar{\mathbf{P}}(\theta) = \mathbf{P}'(\theta)\bar{\mathbf{I}}\mathbf{P}(\theta)$.

C. Direct Position and Speed Estimation

Direct position and speed estimation uses the dynamic model (5) to issue estimates. The numerical performance of the cost function is improved by normalizing the estimates with $\hat{z} = [\hat{\theta}/\Theta, \hat{\omega}/\Omega]'$, where $\Theta = \pi$ is the rated position and $\Omega \in \mathbb{R}_{>0}$ is the base speed. The estimates describe the parameters $z = [\theta/\Theta, \omega/\Omega]'$ with estimation error $\tilde{z} = \hat{z} - z = [\tilde{\theta}/\Theta, \tilde{\omega}/\Omega]'$. The residual function (1) results from (5) defining the state $x = i_{\alpha\beta}$ and input $u = \bar{v}_{\alpha\beta}$,

$$\begin{aligned} r(\hat{z}) = &\left(L_\Sigma \mathbf{I} + L_\Delta \bar{\mathbf{P}}(2\hat{\theta})\right)\dot{i}_{\alpha\beta} \\ &+ 2L_\Delta \hat{\omega}\mathbf{J}\bar{\mathbf{P}}(2\hat{\theta})i_{\alpha\beta} + \hat{\omega}\mathbf{J}\mathbf{P}(\hat{\theta})'\psi_r - \bar{v}_{\alpha\beta} \end{aligned} \tag{6}$$

where $\dot{i}_{\alpha\beta}$, $i_{\alpha\beta}$, and $\bar{v}_{\alpha\beta}$ are known at any sampling instant. The cost function follows immediately by substituting (6) into (2).

The estimation problem (2) is solved numerically in real-time. The solver starts at a guess $\hat{\theta}_g$ and $\hat{\omega}_g$ that is typically chosen as the (extrapolated) estimate of the previous sample. Throughout this research, we use a Newton solver that updates the estimate using the Newton step $\Delta z = \gamma \mathscr{H}_c^{-1}(\cdot)\nabla c(\cdot)$, where $\mathscr{H}_c^{-1}(\cdot) \in \mathbb{R}^{2\times 2}$ is the Hessian and $\nabla c(\cdot) \in \mathbb{R}^2$ is the gradient of the cost and γ is the step-size [22], [23]. The solver stops either when the a convergence criterion is satisfied (typically $\|\nabla c(\cdot)\| \leq \epsilon$ with $\epsilon \in [10^{-2}, 10^{-5}]$) or the maximum number of iterations M is reached (typically $M \in [1,5]$). In practice, the solver may not converge at some samples. In such events, the solver returns the initial guess since $\hat{\theta}^\star = \hat{\theta}_g$ and $\hat{\omega}^\star = \hat{\omega}_g$ is preferable to a random result.

To obtain a meaningful estimate, the cost function must be strictly convex in a neighborhood of the origin, which depends on $\dot{i}_{\alpha\beta}$, $i_{\alpha\beta}$, $\bar{v}_{\alpha\beta}$, and ω. This requirement typically holds, except in steady-state conditions $\dot{i}_{\alpha\beta} = 0$ at $\omega = 0$. To prevent position estimation challenges at $\omega = 0$, a excitation, i.e. perturbation, strategy is required. Popular perturbation strategies are the injection of a pulsating sinusoidal signal along a predefined dq axis [22], [35], [36] or a vector that rotates at high-frequency in the dq space [35], [36]. Since the perturbation is needed only at low speed, the injection magnitude can be reduced as the speed increases to prevent unnecessary losses [37], [38]. Such *periodic perturbation* strategies are beneficial using PWM control. On the other hand, the switching harmonics are visible to control strategies that actuate switching states directly such as direct torque control (DTC) [39], [40] or FCS-MPC [3], [23], [41]. Such controllers never achieve electric steady-state conditions and the inherent *random perturbation* is typically sufficient to estimate position and speed [23], [34]. It is noted that high magnitude, high frequency perturbations tend to drive currents in the magnetic iron and PM. These parasitic currents depend on the motor geometry and result in additional motor losses [42]. Hence, perturbation magnitudes are typically chosen as a compromise between drive system efficiency and estimation robustness (Fig. 2).

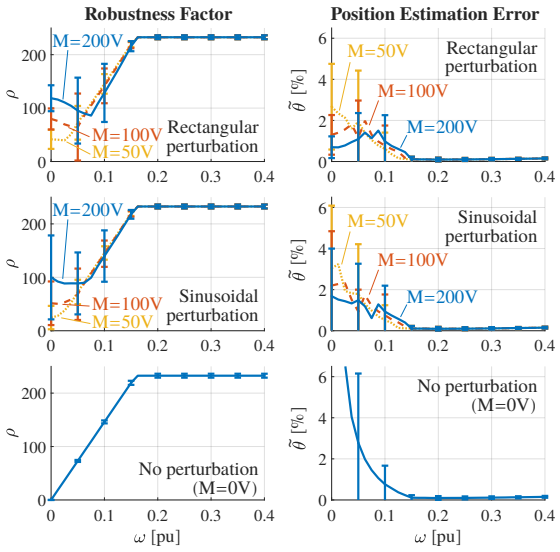

Fig. 2. cost function must be strictly convex in a neighborhood of the origin, which depends on $\dot{i}_{\alpha\beta}, i_{\alpha\beta}, \bar{v}_{\alpha\beta}$, and ω. This requirement typically holds, except in steady-state conditions $\dot{i}_{\alpha\beta} = 0$ at $\omega = 0$. To prevent position estimation challenges at $\omega = 0$, a excitation, i.e. perturbation, strategy is required. Popular perturbation strategies are the injection of a pulsating sinusoidal signal along a predefined dq axis [22], [35], [36] or a vector that rotates at high-frequency in the dq space [35], [36]. Since the perturbation is needed only at low speed, the injection magnitude can be reduced as the speed increases to prevent unnecessary losses [37], [38]. Experimental result: the robustness factor ρ provides an upper error bound against disturbances; the (inverse) correlation with the estimation error is shown on the example of the position error using a (rotating) rectangular, (rotating) sinusoidal, and no perturbation as a function of speed; the perturbation magnitude M is 200V (blue, solid line), 100V (red, dashed line), and 50V (yellow, dotted), i.e. 25%, 12.5%, and 6.25% of the DC voltage, at 0rpm and scaled linearly to zero at 15% of the rated speed

III. Selective and Output Filter Strategies

Direct estimation issues an independent position $\hat{\theta}_k^\star$ and speed $\hat{\omega}_k^\star$ estimate at each sampling instant kT_s, where T_s is the sampling time. The residual $r_k(\cdot)$ and cost $c_k(\cdot) = \|r_k(\cdot)\|^2$ are parameterized with the state $i_{\alpha\beta,k}$, input $\bar{v}_{\alpha\beta,k}$, and state derivative $\dot{i}_{\alpha\beta,k}$, which is typically approximated with $\dot{i}_{\alpha\beta,k} \approx (i_{\alpha\beta,k+1} - i_{\alpha\beta,k})/T_s$.

However, the estimates can be noisy due to any disturbance w, e.g. current sensor noise or inverter nonlinearities such as interlock times or on-voltage drops. Hence, it is beneficial to introduce filtering strategies that maintain the high dynamic performance but prevent that a single "bad" sample results in a large estimation error. We introduce filtering strategies that issue the filtered position $\bar{\theta}_k^\star$ and speed $\bar{\omega}_k^\star$ estimates from $\hat{\theta}_k^\star$ and $\hat{\omega}_k^\star$, which is the result of solving the problem (2).

A. Selective Filtering using Cost Function Properties

The cost function $c_k(\cdot)$ is required to be strictly convex on $\mathscr{D}_k$ such that a meaningful estimate can be issued. Hence, this

concept requires that the cost function is strictly convex in the estimate, or generalizing strongly convex, i.e. $\mathscr{H}_{c_k}(z_k) \geq m_k > 0$, where $m_k = \lambda_{\min}\left(\mathscr{H}_{c_k}(z_k)\right)$ is the minimum eigenvalue of the Hessian evaluated in z_k.

Linearizing the residual $r_k(\cdot)$ in z_k, it is possible to link strength of convexity with the estimation error due to a disturbance. Introducing the robustness factor $\rho_k = \sqrt{m_k}/2$, it can be shown that $\|\tilde{z}_k^\star\| \leq \|w_k\|/\rho_k$ is a tight upper bound on the estimation error. Since the disturbance magnitude is finite, i.e. $\|w_k\| \leq W$, the estimation error magnitude $\|\tilde{z}_k^\star\|$ depends on ρ_k. This property is shown empirically in Fig. 2.

In practice, w_k is unknown. However, the eigenvalues of the cost function m_k and therefore ρ_k are revealed by the Newton solver. Since, samples with low ρ_k have a poor robustness against disturbances, it is feasible to selectively filter samples where $\rho_k < \rho_{min}$. This filtering technique is a simple *if* statement at the output of the solver, which replaces each sample lacking robustness with the initial guess.

B. Finite Impulse Response (FIR) Output Filtering

The problem (2) issues independent estimates $\hat{\theta}_k^\star$ and $\hat{\omega}_k^\star$ at each sampling instant. These estimates are chosen exclusively based on the cost function. However, the mechanical system is subject to constraints as well. For example, the speed cannot vary arbitrarily fast since it is related to kinetic energy stored in the mechanical system. Also, the mechanical parameters should satisfy the equation $\theta_{k+1} = \theta_k + T_s\omega_k$. Hence, it is possible to introduce a moving-window least-squares fit of the estimates over the past N samples, where N is typically small, e.g. a few samples, to limit the computational complexity.

Over short horizons, the speed can often be assumed to be constant without excessive errors [34]. In this research, the speed is assumed to vary linearly over the horizon, i.e. $\hat{\omega}_{k+1}^\star = \hat{\omega}_k^\star + a$, for higher accuracy. This requirement can be written as an equation system that fits the absolute speed

$$\hat{\omega}_k^\star = b \tag{7a}$$
$$\hat{\omega}_{k-1}^\star = b - a \tag{7b}$$
$$\dots \tag{7c}$$
$$\hat{\omega}_{k-N}^\star = b - Na. \tag{7d}$$

It is noted that the assumption of a linear speed variation is exact for $N = \{1, 2\}$ in a sampled system and an approximation (accuracy decreases as N increases), otherwise. It is possible to increase the accuracy by introducing higher order polynomials but at the expense of an increased computation complexity.

Furthermore, the estimates should fit the equation $\hat{\theta}_{k+1}^\star = \hat{\theta}_k^\star + T_s\hat{\omega}_k^\star$. This requirement can be written as an equation system that fits the differential position

$$\hat{\theta}_k^\star - \hat{\theta}_{k-1}^\star = T_s(b - a) \tag{8a}$$
$$\hat{\theta}_{k-1}^\star - \hat{\theta}_{k-2}^\star = T_s(b - 2a) \tag{8b}$$
$$\dots \tag{8c}$$
$$\hat{\theta}_{k-N+1}^\star - \hat{\theta}_{k-N}^\star = T_s(b - Na) \tag{8d}$$

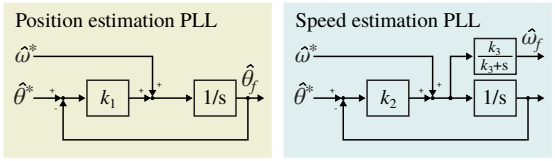

Fig. 3. Dual-PLL structure: a PLL with fast feedback loop (high gain, k_1) is used to achieve a filtered position estimate $\hat{\theta}_f$ with high bandwidth; a PLL with slow feedback loop (low gain, k_2) is used to remove speed offsets with respect to the position increment; a low-pass filter with bandwidth k_3 is used to filter the speed feed-forward term and provides the filtered speed estimate $\hat{\omega}_f$

Finally, the absolute position results from the integration of the speed with initial offset. This system results in the requirement

$$\hat{\theta}_k^\star = c \tag{9a}$$
$$\hat{\theta}_{k-1}^\star = c - T(b - a) \tag{9b}$$
$$\hat{\theta}_{k-2}^\star = c - T(b - a) - T(b - 2a) \tag{9c}$$
$$\dots \tag{9d}$$
$$\hat{\theta}_{k-N}^\star = c - T(Nb - (1 + 2 + .. + N)a). \tag{9e}$$

These systems can be combined and written in matrix form

$$\mathbf{H}\xi = F, \tag{10}$$

where $\xi = [a, b, c]'$ and $F = [\hat{\omega}_k^\star, \dots, \hat{\omega}_{k-N}^\star, \hat{\theta}_k^\star - \hat{\theta}_{k-1}^\star, \dots, \hat{\theta}_{k-N+1}^\star - \hat{\theta}_{k-N}^\star, \hat{\theta}_k^\star, \dots, \hat{\theta}_{k-N}^\star]'$, and

$$\mathbf{H} = \begin{bmatrix} 0 & 1 & 0 \\ -1 & 1 & 0 \\ -2 & 1 & 0 \\ & \dots & \\ -N & 1 & 0 \\ -T_s & T_s & 0 \\ -2T_s & T_s & 0 \\ -3T_s & T_s & 0 \\ & \dots & \\ -NT_s & T_s & 0 \\ 0 & 0 & 1 \\ T_s & T_s & 1 \\ 3T_s & 2T_s & 1 \\ & \dots & \\ \frac{n(n+1)}{2}T_s & NT_s & 1 \end{bmatrix}. \tag{11}$$

The equation system (10) is clearly overdetermined for $N > 0$. Hence, the variable ξ can be fitted in a least-squares sense. The result is provided by $\xi = \mathbf{H}^\dagger F$, where $\cdot^\dagger$ denotes the Moore-Penrose pseudoinverse. The computation is feasible in real-time since $\mathbf{H}$ is constant and $\mathbf{H}^\dagger$ can be stored in memory.

The resulting FIR solves a least-squares problem over a moving horizon N. It issues the fit $\xi = [a, b, c]'$, where $b = \hat{\omega}_{f,k}^\star$ and $c = \hat{\theta}_{f,k}^\star$ are the filtered position and speed, respectively. For $N = 0$, the fit will return the original values $b = \hat{\omega}_{f,k}^\star = \hat{\omega}_k^\star$ and $c = \hat{\theta}_{f,k}^\star = \hat{\theta}_k^\star$.

C. Dual Phase-Locked Loop (PLL)

For large N, the FIR filter can become computationally heavy for real-time implementations since it requires $3N$ floating point multiplications and additions. An alternative is the phase-locked loop (PLL). A PLL tracks the position and co-estimates speed but the latter is typically noisy for high PLL gains, i.e. high PLL bandwidths [3]. However, direct estimation provides both a position and speed signal. Hence, two PLL can be used, one for position and one for speed estimation. A block diagram is shown in Fig. 3. The position-estimation PLL uses the typical

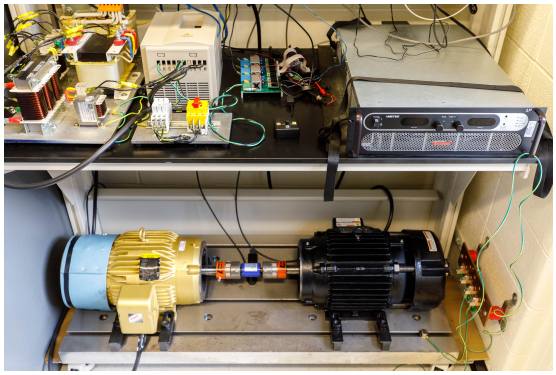

Fig. 4. Experimental PMSM testbench with parameters outlined in Table I

layout augmented with a speed feed-forward term. The position-estimation PLL relies primarily on the $\hat{\theta}^\star$ input to issue a filtered position estimate $\hat{\theta}_f^\star$ with the transfer function

$$\mathrm{tf}_\theta = \frac{\hat{\theta}_f^\star}{\hat{\theta}^\star} = \frac{k_1}{k_1 + s}. \tag{12}$$

The speed-estimation PLL follows the same structure but uses slow feedback ($k_2 \ll k_1$) to remove a speed offset with respect to the position increment. Furthermore, a low-pass filter is added to limit the bandwidth of the speed feed-forward term [3]. The speed-estimation PLL relies primarily on the $\hat{\theta}^\star$ input to issue a filtered position estimate $\hat{\theta}_f^\star$ with the transfer function

$$\mathrm{tf}_\omega = \frac{\hat{\omega}_f^\star}{\hat{\omega}^\star} = \frac{k_3}{k_3 + s}. \tag{13}$$

Throughout this research, we refer to this structure as *dual-PLL*.

The dual-*pll* acts also as a benchmark reference for the FIR filter concept. On the experimental test-bench used in this work, the dual-PLL is stable up to $f_{pll,bw}$ = 1kHz bandwidth, i.e. 1/20 of the sampling frequency, with tuning $k_1 = 2\pi f_{pll,bw}$, $k_2 = 10^{-2}k_1$, and $k_3 = k_1$. In contrast, a conventional PLL is limited to about 50Hz bandwidth due to noise on the speed estimate [22], [23].

IV. Results

The results of this paper have been obtained on the test-bench depicted in Figure 5 with parameters outlined in Table I. The exception is Figure 7, which has been obtained on a software-in-the-loop (SiL) platform, since this dynamic performance study requires an excessive transient load torque, which exceeds the capabilities of the available lab equipment by a factor 10-100 (in bandwidth and magnitude). Instead, the SiL platform executes the same c-code for direct estimation and control but replaces the physical test-bench with a high-fidelity model of the inverter (modeling on-voltage drops and dead-times) and motor (using flux-current maps that capture saturation and cross-saturation). Both, the experimental and SiL platform use peak and valley sampling such that the sampling frequency is twice the switching frequency.

Table I
Motor Drive Parameters

Control and Inverter	
DC voltage	v_c = 800V
Pwm switching period	T_{sw} = 100µs
Sampling period	T_s = 50µs
Interlock time	T_i = 0.3µs
Typical current sensor noise	$I_w \approx 0.5\%$
Microcontroller	200MHz TI C2000 Delfino
Electric Motor	
Base speed	Ω = 1800rpm
Rated torque	T_r = 29.7Nm
Pole pairs	p = 5
Rated current	I_r = 10A
Rated d-axis inductance	L_d = 10.5mH
Rated q-axis inductance	L_q = 12.9mH
Rated PM flux	ψ = 349.1mWb
Rated stator resistance	R = 0.4Ω

All results are obtained using PWM vector control with 1kHz bandwidth. To prevent direct estimation issues at standstill, a rotating voltage perturbation is injected at low speeds. The frequency is chosen to be 5kHz, i.e. 5 times the bandwidth of the current controller to prevent any undesired coupling. Unless otherwise noted, the injection magnitude is chosen to be 120V, i.e. 15% of the DC voltage, at standstill. Increasing the speed $|\omega|$, the injection magnitude is scaled down linearly to zero and no voltage perturbation is applied above 270rpm (absolute speed), i.e. 15% of the rated speed. This perturbation is chosen as a compromise between power losses and robustness based on Fig. 2. Furthermore, all results are obtained without compensating voltage drops $\Delta v_{\alpha\beta}$ in control or estimation to provide a worst-case baseline that can be improved with any compensation technique.

A. Speed-control results

Fig. 5 illustrates the behavior of direct position and speed estimation, where the speed estimate is used for speed control of the machine and the position estimate is used in the inner vector (current) control loop for the Park transformation. The machine follows a speed reference profile with positive and negative speed steps, speed reversal, and finally a step to standstill, where the machine is held. A positive speed, a positive and negative load torque step is applied to illustrate the capability of the speed loop to reject disturbances. The test procedure is used to show the behavior of direct estimation without output filtering (Fig. 5(a)), with FIR filter (Fig. 5(b)) and dual-PLL (Fig. 5(c)). Furthermore, the behavior of selective filtering is illustrated without output filtering (Fig. 5(d)), with FIR filter (Fig. 5(e)) and dual-PLL (Fig. 5(f)). For each test, the following graphs are shown: the reference (blue) and measured (orange) q-axis current (the d-axis current is controlled and remains at zero); the estimated (blue), measured (orange), and reference (yellow) speed; the estimated (blue) and measured (orange) position; the speed error; the position error; and the robustness factor ρ (higher means better rejection of disturbances).

We observe that the direct estimation does not require an output filter and the resulting estimates may be acceptable for some applications. However, the estimates can be noisy since direct estimation issues an independent position and speed estimate at each sampling instant. The error is higher at low speed where the robustness factor tends to be lower (at times zero) and voltage disturbances, e.g. dead-times, or modeling errors result in increased estimation errors. The samples with low robustness factor are removed by selective filtering, which reduces peak

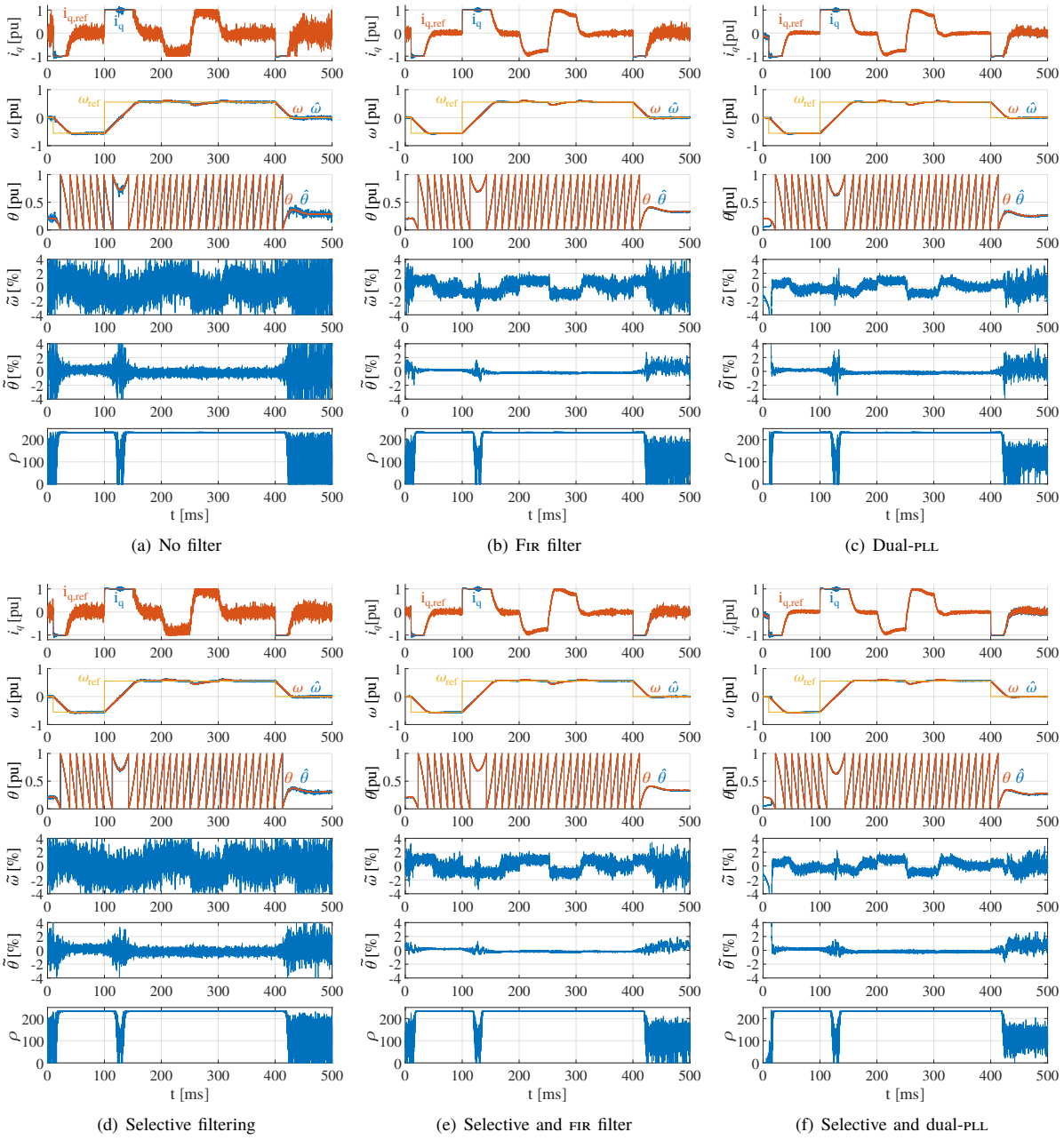

(a) No filter (b) FIR filter (c) Dual-PLL

(d) Selective filtering (e) Selective and FIR filter (f) Selective and dual-PLL

Fig. 5. Experimental result: speed control (-0.60pu step at 10ms, +1.20pu step at 100ms, and -0.60pu step to standstill at 400ms) with load torque steps (+0.75pu at 200ms, -1.5pu at 250ms, and +0.75pu at 300ms): direct position and speed estimation without filter, selective filter with ρ_{min}=50, FIR filter with N=10, dual-PLL with 1kHz position and speed bandwidth, and combinations thereof. Each figure traces the following graphs (top to bottom): measured i_q and reference $i_{q,\text{ref}}$ current; measured ω, estimated $\hat{\omega}$, and reference ω_{ref} speed; measured θ and estimated $\hat{\theta}$ position; speed error $\tilde{\omega}$; position error $\tilde{\theta}$; robustness factor ρ.

estimation errors, which is especially noticeable in the position error. Both approaches can be combined with FIR and dual-PLL filtering. The FIR results are reported using $N = 10$ samples for filtering. The dual-PLL was tuned to the highest stable bandwidth on the test-bench, which corresponds to 1kHz. In comparison, the FIR filter results in a cleaner position estimate but increased speed estimation noise (while achieving a higher bandwidth, see Subsection IV-B).

B. Dynamic filter performance

The dynamic performance of direct estimation with output filters is evaluated by setting the estimator (and filters) to an erroneous estimate and measuring the convergence times to the correct values. The Fig. 6 shows the convergence from a 10% position estimation error at t=1ms, 10% speed estimation error at t=2ms, and 10% position and speed estimation error t=3ms. These tests are used to evaluate the practical bandwidth $pbw = 0.34/t_r$, where t_r is the 10% to 90% rise time [41]. It is observed that without output filter, direct estimation corrects a position or speed error within one sample, which corresponds to 6.8kHz practical bandwidth on the test system with 20kHz sampling frequency. The output filters reduce the noise on the estimates at the expense of dynamic performance. On position errors, the FIR filter has a

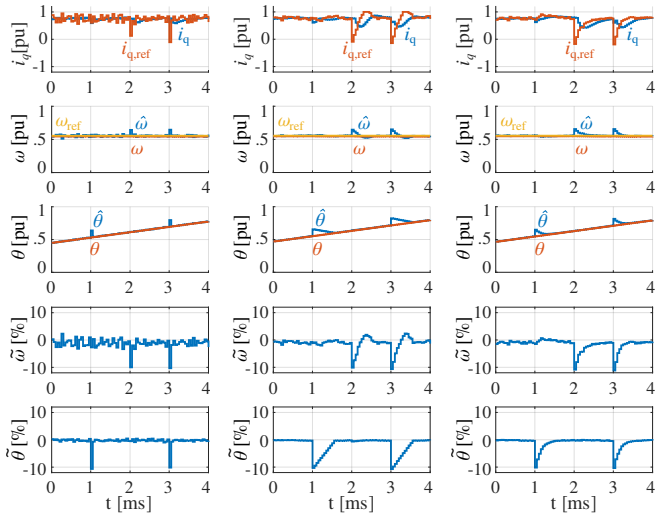

(a) No output filter (b) FIR filter (c) Dual-PLL filter

Fig. 6. Experimental result: convergence of direct position and speed estimation using selective filtering with ρ_{min}=50 without output filter, with FIR filter with N=10, and with dual-PLL with 1kHz position and speed bandwidth from an erroneous setpoint: 10% position estimation error at t=1ms, 10% speed estimation error at t=2ms, and 10% position and speed estimation error t=3ms. Each figure traces the following graphs (top to bottom): measured i_q and reference $i_{q,\text{ref}}$ current; measured ω, estimated $\hat{\omega}$, and reference ω_{ref} speed; measured θ and estimated $\hat{\theta}$ position; speed error $\tilde{\omega}$; position error $\tilde{\theta}$.

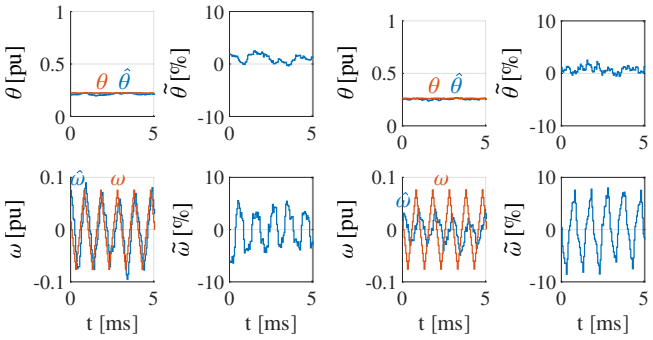

(a) FIR and selective filter (b) Dual-PLL and selective filter

Fig. 7. Result obtained on the software-in-the-loop platform: dynamic performance in presence of a zero-mean 1kHz triangular speed variation (driven by an unrealistic load torque): direct position and speed estimation using selective filtering with ρ_{min}=50 combined with FIR filter with N=10 and dual-PLL with 1kHz position and speed bandwidth. Each figure traces the following graphs: measured θ and estimated $\hat{\theta}$ position; measured ω and estimated $\hat{\omega}$ speed; position error $\tilde{\theta}$; speed error $\tilde{\omega}$.

t_r of 8 samples, which results in 0.85kHz practical bandwidth. This behavior is expected since the FIR filter converges linearly by design (at constant speed) and must replace 80% of the N internally stored "erroneous" samples to reduce the error by 80%. The dual-PLL filter has a t_r of 7 samples, which results in 0.97kHz. This result corresponds to the design bandwidth of 1kHz and the filter has the expected exponential decay of a first-order filter. On speed errors, the FIR filter has a t_r of 3 samples, which results in 2.3kHz practical bandwidth. In this case, the FIR filter is faster as it fits both the position and speed estimate and a speed sequence with offset does not fit the expected position increment. In contrast, the dual-PLL filter relies predominantly on the speed estimate and has a t_r of 7-8 samples, which results in 0.85kHz-0.97kHz. Both filters behave similarly when a position and speed error occurs simultaneously. It is noted that the practical bandwidth of the FIR filter can be increased by decreasing N, where N=0 corresponds to a pass-through without filtering (see Subsection IV-D). On the other hand, increasing the bandwidth of the dual-PLL filter resulted in stability issues.

As a second test, the dynamic performance of direct estimation is evaluated by applying an excessive (400Nm) transient (1kHz) load torque signal, which exceeds the induction-machine dyno capabilities by a factor 10 in magnitude and bandwidth. Hence, the results presented in Fig.7 are obtained on the SiL platform. The load torque is applied to achieve a $\pm$10% 1kHz speed variation at zero speed, where the estimation robustness tends to be low (see Subsection IV-A). The tests are performed using selective filtering combined with FIR filter and dual-PLL. In direct comparison, the FIR filter traces the high-frequency speed signal significantly better. In fact, it achieves more than twice the speed estimation bandwidth (with N=10), which can be further increased, while achieving a similar filter performance (see Subsection IV-A)). This test is performed since speed estimation bandwidth has a high priority in many practical applications. The speed signal is the measured, i.e. estimated, input of the speed control loop, which is a common configuration and may require high bandwidths (especially if an external, cascaded position loop is used). Furthermore, a high bandwidth speed signal can provide useful information on the load torque dynamics or torque ripples.

C. Selective filter evaluation

The selective filter performance is evaluated at zero speed where the robustness factor ρ tends to be low. Fig. 8 presents the results for multiple runs plotted with respect to the minimum robustness factor ρ_{min}. Hence, the direct estimation algorithm does not issue a new estimate when $\rho < \rho_{min}$ but extrapolates the measurement from the previous sampling instant.

A small ρ_{min} improves the mean, worst-case, and RMS position and speed estimation error considerably compared to $\rho_{min} = 0$. Increasing ρ_{min} reduces the errors marginally. However once ρ_{min} is larger than the mean ρ value, the estimation process deteriorates quickly since a majority of the samples are discarded.

Finally, it is noted that the computational overhead of selective filtering is irrelevant. Direct estimation typically uses a Newton method for identifying the estimates [22], [23]. Hence, it exposes the 2×2 Hessian of the cost function, which is needed in the Newton step. Numerical instabilities are prevented using an eigenvalue check, which is trivial for a matrix of this size. Upon convergence, the solver can simply check the resulting ρ and discard the estimate if needed. These checks can be performed in <10ns.

D. FIR filter evaluation

The FIR filter performance is evaluated at zero speed where the estimation noise tends to be high. Fig. 9 presents the results for multiple runs plotted with respect to the number of samples N that are used for filtering. As expected, increasing the number of samples improves the mean, worst-case, and RMS position and speed estimation error. Initially the increase is significant and the estimation errors are approximately halved at $N = 10$ (compared

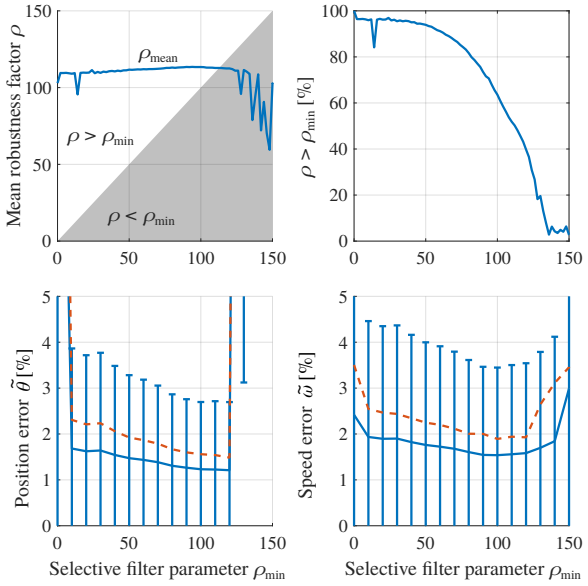

Fig. 8. Experimental result: selective filtering behavior with respect to filter parameter ρ_{min} at standstill (the robustness factor ρ is lowest at $\omega = 0$rpm on average): some ρ_{min} improves the mean, worst case, and RMS (dashed) estimation errors, excessive ρ_{min} tends to filter a majority of the estimates, which compromises the estimation process.

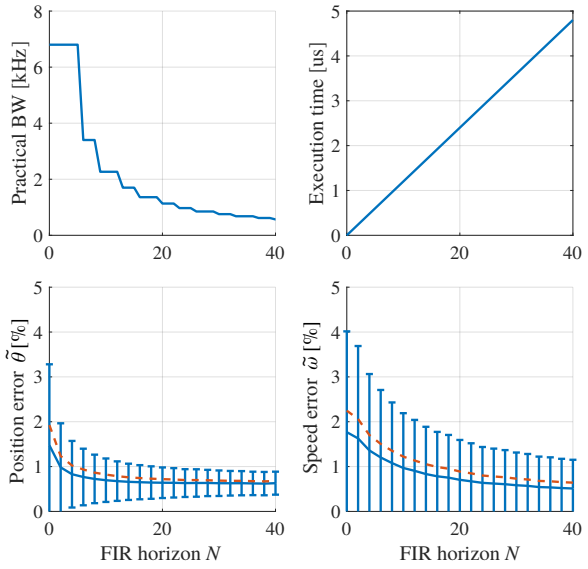

Fig. 9. Experimental result: FIR filter behavior with respect to length N at standstill (the robustness factor ρ is lowest at $\omega = 0$rpm on average): increasing N increases the signal stability against estimation noise (except offsets e.g. due to modeling errors) at the expense of reducing the practical bandwidth ($pbw = 0.34/t_r$, where t_r is the 10% to 90% rise time of the speed estimate [41]) and increasing the computation time.

to $N = 0$). However, the improvements tend to level out at high N. This behavior is expected since output filters are effective in removing noise. The remaining offset, which may result from modeling errors, is found to be <1%.

Increasing the filtering performance, i.e. N, is expected to reduce the filter dynamics, i.e. bandwidth. This behavior is quantified using the concept of practical bandwidth $pbw = 0.34/t_r$, where t_r is the 10% to 90% rise time [41]. An estimation offset is introduced and the "rise time" is measured until the estimate falls below 10% of the initial error. The maximum achievable pbw is 6.8kHz since direct estimation without output filter ($N = 0$) requires at least 1 sample ($50\mu s$) to reach the estimate. The pbw remains at 6.8kHz for $N \in [0, 5]$, 4.3kHz for $N \in [6, 8]$, 2.3kHz for $N = [9, 12]$. By comparison the dual-PLL is unstable at frequencies exceeding 1kHz on the used test-bench configuration. Tuned to 1kHz, it achieves estimates with a similar noise compared to the FIR filter with $N = 10$ and more than double the bandwidth.

Finally, the computation complexity of the FIR filter increases linearly with N. However, typical values, e.g. up to $N = 20$, remains trivial to execute on typical motor drive microcontrollers.

V. Conclusion

This paper studies high-performance filter strategies for direct position estimation since estimates can be affected by disturbances and noise. Two types of filters are proposed, a selective filter strategy that evaluates the robustness of an estimate against noise and discards estimates lacking robustness. The concept is found to be effective against worst case estimation errors, which are reduced by a factor of approximately 4. Hence, some selective filtering should always be applied.

The output filters store past samples and use them for filtering. Since direct estimation issues an independent position and speed estimate, both estimates are used for filtering. A finite impulse response (FIR) filter is proposed that fits the past N samples according to a least squares criterion. This approach decreases the estimation noise with no compromise in terms of dynamics up to $N = 5$ and a limited decrease of dynamics at higher N. At the test bench the practical bandwidth is found to be 6.8kHz for $N \in [0, 5]$, 4.3kHz for $N \in [6, 8]$, and 2.3kHz for $N \in [9, 12]$.

Furthermore, a dual-PLL output filter is proposed and evaluated. The concept achieves a 1kHz bandwidth compared to about 50Hz of a conventional PLL and acts as a benchmark reference for the FIR filter. Hence, direct estimation with FIR or dual-PLL output filters can achieve a 10 to 100 times higher bandwidth than a conventional PLL at the same absolute mean error (<1%). Furthermore, the FIR has 5 times the bandwidth of the dual-PLL at a similar noise. Finally, the computational complexity of the filters is evaluated and the execution time (a few microseconds) is considered negligible in typical settings.

References

[1] S. Morimoto *et al.*, "Sensorless control strategy for salient-pole PMSM based on extended EMF in rotating reference frame," *IEEE Trans. Ind. Appl.*, vol. 38, pp. 1054–1061, 2002.

[2] Z. Chen *et al.*, "An extended electromotive force model for sensorless control of interior permanent-magnet synchronous motors," *IEEE Trans. Ind. Electron.*, vol. 50, pp. 288–295, 2003.

[3] M. Preindl and E. Schaltz, "Sensorless model predictive direct current control using novel second-order PLL observer for PMSM drive systems," *IEEE Trans. Ind. Electron.*, vol. 58, pp. 4087–4095, 2011.

[4] M. H. Bierhoff, "A general pll-type algorithm for speed sensorless control of electrical drives," *IEEE Transactions on Industrial Electronics*, vol. 64, pp. 9253–9260, 2017.

[5] S. Shinnaka, "New sensorless vector control using minimum-order flux state observer in a stationary reference frame for permanent-magnet synchronous motors," *IEEE Trans. Ind. Electron.*, vol. 53, pp. 388–398, 2006.

[6] T. Chan *et al.*, "Sensorless permanent-magnet synchronous motor drive using a reduced-order rotor flux observer," *IET Electr. Power Appl.*, vol. 2, pp. 88–98, 2008.

[7] S. Chi *et al.*, "Sliding-mode sensorless control of direct-drive PM synchronous motors for washing machine applications," *IEEE Trans. Ind. Appl.*, vol. 45, pp. 582–590, 2009.

[8] G. Wang *et al.*, "Quadrature PLL-based high-order sliding-mode observer for IPMSM sensorless control with online MTPA strategy," *IEEE Trans. Energy Convers.*, vol. 28, pp. 214–224, 2013.

[9] S. Bolognani *et al.*, "Sensorless full-digital PMSM drive with EKF estimation of speed and rotor position," *IEEE Trans. Ind. Electron.*, vol. 46, pp. 184–191, 1999.

[10] Y.-H. Kim and Y.-S. Kook, "High performance IPMSM drives without rotational position sensors using reduced-order EKF," *IEEE Trans. Energy Convers.*, vol. 14, pp. 868–873, 1999.

[11] M. Montanari *et al.*, "Speed sensorless control of induction motors based on a reduced-order adaptive observer," *IEEE Trans. Control Syst. Technol.*, vol. 15, pp. 1049–1064, 2007.

[12] J. Choi *et al.*, "Robust adaptive sensorless control for permanent-magnet synchronous motors," *IEEE Trans. Power Electron.*, vol. 32, pp. 3989–3997, 2017.

[13] S. Bolognani *et al.*, "Sensorless control of IPM motors in the low-speed range and at standstill by HF injection and DFT processing," *IEEE Trans. Ind. Appl.*, vol. 47, pp. 96–104, 2011.

[14] S. Kim *et al.*, "PWM switching frequency signal injection sensorless method in IPMSM," *IEEE Trans. Ind. Appl.*, vol. 48, pp. 1576–1587, 2012.

[15] R. Antonello *et al.*, "Enhanced low-speed operations for sensorless anisotropic pm synchronous motor drives by a modified back-emf observer," *IEEE Transactions on Industrial Electronics*, vol. 65, pp. 3069–3076, 2018.

[16] L. Rovere *et al.*, "Sensorless finite-control set model predictive control for ipmsm drives," *IEEE Trans. Ind. Electron.*, vol. 63, pp. 5921–5931, 2016.

[17] V. Muzikova *et al.*, "Finite control set MPC with high frequency injections for sensorless position and speed estimation of a PMSM," in *IEEE PRECEDE*, IEEE, 2015.

[18] G.-D. Andreescu *et al.*, "Combined flux observer with signal injection enhancement for wide speed range sensorless direct torque control of IPMSM drives," *IEEE Trans. Energy Convers.*, vol. 23, pp. 393–402, 2008.

[19] G. Wang *et al.*, "DSP-based control of sensorless IPMSM drives for wide-speed-range operation," *IEEE Trans. Ind. Electron.*, vol. 60, pp. 720–727, 2013.

[20] F. Genduso *et al.*, "Back EMF sensorless-control algorithm for high-dynamic performance PMSM," *IEEE Trans. Ind. Electron.*, vol. 57, pp. 2092–2100, 2010.

[21] G. Zhang *et al.*, "Adaline-network-based pll for position sensorless interior permanent magnet synchronous motor drives," *IEEE Transactions on Power Electronics*, vol. 31, pp. 1450–1460, 2016.

[22] Y. Sun *et al.*, "Unified wide speed range ipm sensorless scheme using nonlinear optimization," *IEEE Trans. Power Electron.*, vol. 32, pp. 6308–6322, 2017.

[23] S. Nalakath *et al.*, "Optimization-based position sensorless finite control set model predictive control for ipmsms," *IEEE Trans. Power Electron.*, vol. 33, pp. 8672–8682, 2018.

[24] X. Yong and M. Preindl, "Optimization-based position estimation of pm synchronous machine motor drives with magnetic saturation," in *IEEE SLED*, 2018.

[25] A. D. Callegaro *et al.*, "Optimization-based position sensorless for induction machines," in *IEEE ITEC*, 2018.

[26] B. Nahid-Mobarakeh *et al.*, "Mechanical sensorless control of PMSM with online estimation of stator resistance," *IEEE Trans. Ind. Appl.*, vol. 40, pp. 457–471, 2004.

[27] B. Nahid-Mobarakeh *et al.*, "Back EMF estimation-based sensorless control of PMSM: Robustness with respect to measurement errors and inverter irregularities," *IEEE Trans. Ind. Appl.*, vol. 43, pp. 485–494, 2007.

[28] P. Guglielmi *et al.*, "Cross-saturation effects in IPM motors and related impact on sensorless control," *IEEE Trans. Ind. Appl.*, vol. 42, pp. 1516–1522, 2006.

[29] H. Machida *et al.*, "A motor speed control system using a hybrid of dual-loop pll and feed-forward," in *IEEE International Workshop on Advanced Motion Control (AMC)*, 2010.

[30] H. Mchida *et al.*, "A motor speed control system using dual-loop pll and speed feed-forward/back," in *IEEE International Conference on Mechatronics and Automation*, 2010.

[31] Yituo Li *et al.*, "A novel sensorless control method of ipmsm using dual pll structure," in *International Power Electronics and Motion Control Conference*, 2012.

[32] G. Giorgi *et al.*, *Mathematics of Optimization: Smooth and Nonsmooth Case*. Elsevier Science, 2004.

[33] M. Preindl and S. Bolognani, "Optimal state reference computation with constrained MTPA criterion for PM motor drives," *IEEE Trans. Power Electron.*, vol. 30, pp. 4524–4535, 2015.

[34] M. Preindl, "Robust control invariant sets and lyapunov-based mpc for ipm synchronous motor drives," *IEEE Trans. Ind. Electron.*, vol. 63, pp. 3925–3933, 2016.

[35] N. Bianchi *et al.*, "Comparison of pm motor structures and sensorless control techniques for zero-speed rotor position detection," *IEEE Trans. Power Electron.*, vol. 22, pp. 2466–2475, 2007.

[36] D. Raca *et al.*, "Carrier-signal selection for sensorless control of pm synchronous machines at zero and very low speeds," *IEEE Trans. Ind. Appl.*, vol. 46, pp. 167–178, 2010.

[37] S. Nalakath *et al.*, "Modeling and analysis of core loss of an ipm machine for online estimation purposes," in *IEEE IECON*, 2015.

[38] Y. Yang *et al.*, "Thermal management of electric machines," *IET Electr. Syst. Transp.*, vol. 7, pp. 104–116, 2017.

[39] I. Takahashi and T. Noguchi, "A new quick-response and high-efficiency control strategy of an induction motor," *IEEE Trans. Ind. Appl.*, vol. IA-22, pp. 820–827, 1986.

[40] M. Depenbrock, "Direct self-control of inverter-fed induction machine," *IEEE Trans. Power Electron.*, vol. 3, pp. 420–429, 1988.

[41] M. Preindl and S. Bolognani, "Model predictive direct torque control with finite control set for PMSM drive systems, part 1: Maximum torque per ampere operation," *IEEE Trans. Ind. Inf.*, vol. 9, pp. 1912–1921, 2013.

[42] S. Yang and R. D. Lorenz, "Analysis of iron and magnet losses in surface-permanent-magnet machines resulting from injection-based self-sensing position estimation," *IEEE Transactions on Industry Applications*, vol. 48, pp. 1901–1910, 2012.

Matthias Preindl (S'12-M'15-SM'18) received the B.Sc. degree in electrical engineering (*summa cum laude*) from the University of Padua, Italy, the M.Sc. degree in electrical engineering and information technology from ETH Zurich, Switzerland, and the Ph.D. degree in energy engineering from the University of Padua, in 2008, 2010, and 2014, respectively. He was an R&D Engineer of Power Electronics and Drives at Leitwind AG, Italy (2010-2012), a Post Doctoral Research Associate with the McMaster Institute for Automotive Research and Technology, McMaster University, Hamilton, ON, Canada (2014-2015), and a Sessional Professor in the Department of Electrical and Computer Engineering, McMaster University (2015). He is currently an Assistant Professor in the Department of Electrical Engineering at Columbia University, USA. He received several awards and honors including the Horiba Awards Honorable Mention (Japan, 2019), the Futura Foundation Award (Italy, 2017), the NSF CAREER Award (USA, 2017), and he is the co-recipient of several best paper and presentation recognitions.